



Upper Paleocene–lower Eocene calcareous nannofossil biostratigraphy at Nukhul, West Central Sinai, Egypt

Atef M. Kasem¹ · Walid G. Kassab²

Received: 30 August 2023 / Accepted: 3 November 2023
© The Author(s) 2023

Abstract

This research offers a comprehensive examination of calcareous nannofossils, isotopic ratios ($\delta^{18}\text{O}$ and $\delta^{13}\text{C}$), and carbonate content spanning the critical Paleocene-Eocene transition at Gebel Nukhul. The study covers three lithostratigraphic formations: Tarawan, Esna, and Thebes. By meticulous analysis, we've identified five distinct calcareous nannofossil zones, including NP7/8 and NP9-12. Zone NP9 is further divided based on the lowest occurrences of specific nannofossils (*Discoaster anartios*, *D. araneus*, and/or *Rhombaster* spp.), while Zone NP10 is subdivided using *Tribrachiatius contortus* as a marker. We discussed the significance of various calcareous nannofossil taxa in biostratigraphy, highlighting their role as valuable stratigraphic markers. Our research precisely locates the base of the Eocene at the onset of Subzone NP9b within the Esna Formation, revealing no discernible lithological changes coinciding with this boundary. Additionally, our findings align with the global record, indicating significant decreases in $\delta^{13}\text{C}$, $\delta^{18}\text{O}$, and calcium carbonate (CaCO_3) content during the Paleocene–Eocene transition. These changes underscore the climatic and environmental perturbations during this pivotal geological phase. This study provides valuable insights into the stratigraphy and paleoclimatology of the Paleocene–Eocene transition, contributing to our understanding of past climatic variations on Earth.

Keywords Calcareous nannofossils · Biostratigraphy · Carbon and oxygen isotopes · Paleocene–Eocene boundary · *Sphenolithus* · *Rhombaster*

1 Introduction

Paleocene–Eocene (P–E) was a crucial interval, during which global paleontological and isotopic changes took place. It was marked by a short (170–220 kyr) and extremely warm period that resulted in various biotic and isotopic changes [11, 18, 25, 26, 40]. Several Egyptian sections provide valuable biotic and chemical data through P–E because Egypt existed at the Tethys Sea's margin during the early Tertiary [31, 32].

The Global Stratotype Section and Point (GSSP) for Eocene was placed at Dababiya in south Egypt [18]. At

the beginning of the carbon isotope excursion (CIE) that has been globally documented, the Eocene started at Dababiya. It was accompanied by benthonic foraminifera' major demise [43] and coincides with the marker beds [18]. These beds are known as Dababiya Quarry Beds and are marked by mineralogical, chemical, and paleontological characteristics. They were documented from numerous localities in Egypt [25, 26, 33, 42]. Further subdivision was suggested for these beds [9].

Calcareous nannofossils are valuable in recognition of biotic variations through the Paleocene–Eocene because they are sensitive to environmental changes as well as their complete record along this time (see [25, 26] for more references). This study includes (1) a lithological description of the uppermost Paleocene–lowermost Eocene at Nukhul (2) carrying out biozonation based on calcareous nannofossils and revealing variations of their assemblages, in addition to (3) revealing changes of carbonate contents as well as $\delta^{18}\text{O}$ and $\delta^{13}\text{C}$ values through the Paleocene–Eocene transition.

✉ Atef M. Kasem
Kasematef@yahoo.com; kasematef@sci.dmu.edu.eg
Walid G. Kassab
wkassab@cu.edu.eg

¹ Geology Department, Faculty of Science, Damanhour University, Damanhour, Egypt

² Geology Department, Faculty of Science, Cairo University, Cairo, Egypt

2 Location, materials and methods

Collection of 66 rock samples was achieved from the P–E at Nukhul (Lat. 29° 04' 46" N—Long. 33° 10' 21" E), which is located in western Central Sinai (Fig. 1). For calcareous nannofossil investigation, pipette strew slides were prepared for each sample. To ensure approximately equal weight of sediments per same area of cover slip for all samples, the following procedures were followed:

1. The sediments were dried in an oven to allow accurate weighing of the sample and help the disaggregation of clay-rich samples.
2. A subsample of about 0.1 gm of dry sediment was weighted from each sample using a microbalance with precision of 0.001 gm, and transferred into beaker, a 10 ml test tube.
3. A 10 ml of distilled water had been added and shaking was carried out for dispersion of the sediments.

4. A 0.25 mm of the well-mixed solution was pipetted onto a 22×22 mm coverslips, ensuring that it covers the entire surface then it had been dehydrated on a hotplate.
5. D.P.X mountant was used to mount the coverslip onto a slide.

A Zeiss Axio-Photo light microscope was used to examine smear slides. About 50 fields of view on the slide were examined and specimens were counted to recognize their relative abundances.

Calcium carbonate contents, $\delta^{13}\text{C}$ and $\delta^{18}\text{O}$ analyses had been achieved at University of Florida, USA. Coulometrical measurements of inorganic carbon were carried out on 54 rock samples [19]. An isotope ratio mass spectrometer (Finnigan-MAT 252) had been utilized for measurement of carbon and oxygen isotopes. Isotopic data were recorded comparative to Vienna Pee Dee Belemnite (VPDB, [17]). These analyses were performed with a precision of $\pm 0.040\text{‰}$ for d^{13}C and 0.072‰ for d^{18}O ($n=33$).

Fig. 1 Location map of Nukhul section



3 Lithostratigraphy

The sturdy interval covers the following stratigraphic units (Fig. 2):

3.1 The Tarawan Formation

At G. Tarawan (Kharga Oasis, Egypt) this formation is an interval of chalk changes upward to chalky limestones and then marly limestone [10]. At Nukhul, the uppermost

Tarawan F. (~2m) is included. It consists of yellowish-chalky limestone (Fig. 2) and is assigned to the Thanetian Epoch.

3.2 The Esna Formation

It had been distinguished by Beadnell [12] to characterize a shale sequence, which has calcareous intercalations and grades into argillaceous limestone in between the upper Cretaceous and Eocene successions at G. Oweina close to Esna, Egypt. Subsequently, Said [38] designate this unit Esna F. At Nukhul, the Esna F. is about 25 m thick of dark

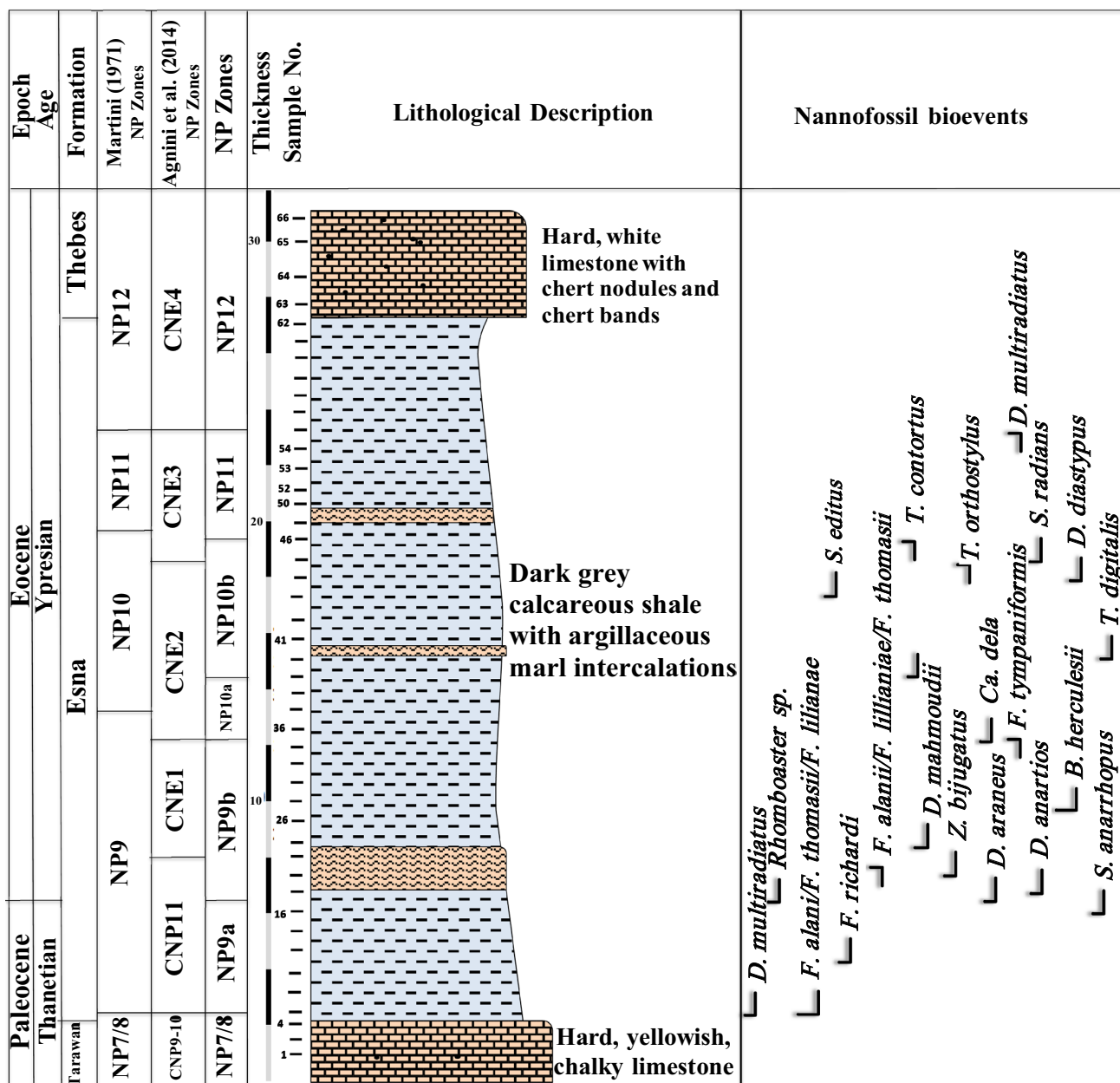


Fig. 2 Lithostratigraphic columnar section of the late Paleocene–early Eocene sequence at the Nukhul section, West Central Sinai, Egypt

grey calcareous shale with argillaceous marl intercalations (Fig. 2). It was dated as Thanetian-Ypresian. Several authors subdivided the Esna Formation into various units (see [26] for more discussion). The DQB's that associate with the Eocene's base GSSP were not documented in the present study (Fig. 2).

3.3 The Thebes Formation

Said [38] appointed it to mark a 290 m limestone bed with numerous flint bands overlies the Esna F. at Gabal Gurnah, Nile Valley, Egypt. At Nukhul, about 4 m of Thebes F. were examined. It consists of limestone (hard and white) with chert nodules and bands (Fig. 2). This interval was assigned to the Ypresian Epoch.

4 Biostratigraphy

In this study, the zonation scheme of Martini [28] was adopted. Zone NP7 plus Zone NP8 were gathered following Romein's [37] suggestion. Further subdivision of Zones NP9 in addition to NP10 was adopted. Stratigraphic distributions of nannofossil assemblages are shown in the Table 1. Recognized zones and subzones are discussed as follows.

4.1 Zone NP7/8

Hay [23] introduced *Discoaster mohleri* Zone using the LO of *Heliolithus riedelii* as a marker to the start of this zone. However, *H. riedelii* was considered an unreliable biostratigraphic marker [34], thus Romein [37] combined Zones NP7 plus NP8 into Zone NP7/8 that span from the LOs of *D. mohleri* to *D. multiradiatus*. *Discoaster mohleri* Zone belongs to Thanetian Age [4]. At Nukhul, Zone NP7/8 extends from samples 2–5 in the Tarawan F. (Fig. 2 and table), and is assigned to Thanetian Epoch.

4.2 Zone NP9

Bramlette and Sullivan [14] introduced this zone that was revised by Martini [28]. The LO of *Discoaster multiradiatus* delineates its base and the LO of *Tribrachiatus bramlettei* delineates its top. Several studies in Egypt recorded this zone ([25, 26] for more references). At Nukhul, *D. multiradiatus* first occurred in sample 6 (Table), and *T. bramlettei* first occurred with continuous occurrence in sample 35. In this study, the LCtO of *T. bramlettei* is adopted to recognize the upper limit of Zone NP9. It has about 10 m thickness and its base matches with the starting of Esna F. (Fig. 2). *Rhomboaster* first appears and radiate in this zone. Paleocene *Fasciculiths* and *Discoaster* taxa appear and radiate in this zone (Table). *Campylosphaera dela* had been used to further

divide the interval equivalent to Zone NP9 [16], however, later studies confirmed its unreliability for biostratigraphic zonation and correlation [25]. Zone NP9 was further subdivided into Subzones NP9a as well as NP9b [8]. This proposition had been followed in this study (Table).

4.2.1 NP9a Subzone

The LOs of *Discoaster multiradiatus* mark its beginning and *Rhomboaster* spp., *D. anartios* and/or *D. araneus* that mark its top [8]. At Nukhul, this subzone extends from samples 6 to 16 and has a thickness of 4 m in the lowermost of the Esna F. and has been assigned to Thanetian Age (Fig. 2).

4.2.2 NP9b Subzone

The top of this subzone is delineated by the LO of *Tribrachiatus bramlettei* [8]. At Nukhul, it covers samples 17 to 34 and is about 5.8 m thick and has been designated to Ypresian Epoch (Fig. 2). Numerous species first appear in this interval including: *D. araneus*, *R. cuspis*, *R. calcitrapa*, *R. bitrifida*, *D. anartios*, *T. spineus*, *Blackites herculesii*, *D. salisburgensis*, *D. mahmoudii*, *Pontosphaera exilis*, *Zygrhablithus bijugatus*, *D. paelikei*, *Helicosphaera seminulum*, *D. binodus*, *Pontosphaera ocellata*, *P. multipora*, and *D. splendidus*.

4.3 *Tribrachiatus contortus* zone (NP10)

The LO of *Tribrachiatus bramlettei* delineates its base whereas its top is marked by the HO of *T. contortus* [23]. In this study it extends from samples 35 to 46 and is about 7.5 m within the Esna F. and is designated to Ypresian Epoch (Fig. 2). The structure of *Tribrachiatus bramlettei* and *Rhomboaster* is considered different by some authors [25]. Thus, Faris et al. [22] recommended identifying Zone's NP10 base by the common occurrence of *T. bramlettei*. In this study, *T. bramlettei* appears in samples 24, 25 and 27 with rare occurrence and began to appear continuously in sample 35 and in common occurrence in sample 38. The reliability of further subdivision of this zone based on the LOs and HOs of *Tribrachiatus contortus* and *T. digitalis* had been assured by several studies (see [42] for more references). However, the range of *T. digitalis* and its systematic position were criticized [35]. Therefore, Zone NP10 was further subdivided into two subzones using the LO *T. contortus* [25]. The overlapping ranges of *T. bramlettei*—*T. contortus*, in addition to overlapping ranges of *T. contortus*—*T. orthostylus* indicate that Zone NP10 is complete [42]. At Nukhul, *T. bramlettei* overlaps in range with *T. contortus* in Zone NP10 (samples 39–42). Furthermore, an overlapping in ranges of *T. contortus*—*T. orthostylus* was documented in Zone NP10 (sample 45 to sample 46) (Table).

4.3.1 NP10a subzone

Appearing of *Tribrachiatus bramlettei* marks the base of this subzone and the LO of *T. contortus* marks its top [25]. It is equivalent to Subzones NP10a and NP10b of Tantawy [41]. It is ~2 m thick at the Nukhul section (Fig. 2) covering samples 35 to 38 within the Esna F. It is assigned to Ypresian Epoch (Table).

4.3.2 Subzone NP10b

This zone spans the whole extent of *Tribrachiatus contortus* [25]. It is equivalent to Subzone NP10c of Tantawy [41]. It has a thickness of 5 m (Fig. 2), and belongs to Ypresian Epoch. *Tribrachiatus digitalis* appears in sample 40 within this subzone just above the appearance of *T. contortus* (Table).

4.4 Zone NP11

It extends between the HO and LO of *Tribrachiatus contortus* and *Discoaster lodoensis*, respectively [24]. It covers about 4 m of the Esna F. at Nukhul (Fig. 2). It is assigned to Ypresian Age. *Tribrachiatus orthostylus* often appears slightly below the boundary between Zones NP10 and NP11 and, thus, approximate the top of Zone NP10 [34]. Moreover, appearances of *Sphenolithus radians* plus *T. orthostylus* are synchronized [3, 25]. A similar finding was recorded in this study that confirms their stratigraphic reliability in approximating the top of Zone NP10.

4.5 Zone NP12

It extend between the LO and HO of *Discoaster lodoensis* and *Tribrachiatus orthostylus*, respectively [15]. At Nukhul, it has 4 m thickness and extends across the Esna—Thebes Formations (Fig. 2).

5 Discussion

Throughout the Paleocene and Eocene, striking lithological, chemical, and biotic changes were discovered. According to Dupuis et al. [18], these modifications have a major impact on how the P-E boundary and regional correlations are recognized. Numerous sections have described changes in the assemblage of calcareous nannofossils in Egypt throughout this time (see [6, 7, 27, 40] for further references). The base of Eocene was placed within Zone NP9, within Zone NP10 or at the boundary between Zones NP9 and NP10 (see [25] for more references). At the Dababiya GSSP, it synchronizes Subzone's NP9b base [18].

Calcareous nannofossil excursion taxa (CNET) are the most important guide that characterizes Eocene's base at the Dababiya GSSP [13]. They include *Rhombaster* spp., *Discoaster araneus*, plus *D. anartios*. Irregular length and asymmetrical arrangement of rays of these taxa refers to unusual conditions as reported by Mutterlose et al. [30]. Yet the lowermost Eocene interval (~73 cm) at the GSSP is barren of carbonate and overlain by strata contain CNET [18]. Thus, their rigorous ranges are unknown. At Nukhul, the Eocene's base matches the beginning of Subzone NP9b. No lithological change is documented at this boundary at the Nukhul section.

The LO of *Tribrachiatus bramlettei* is valuable in biostratigraphy [28]. Studies documented discontinuous and rare to very rare occurrences of *T. bramlettei* just on top of the CIE and the LO of *Rhombaster* spp. [2, 3]. Moreover, Agnini et al. [3] reported that calibrations show inconsistent beginnings of *T. bramlettei*. These inconsistencies are probably consequence of diachrony, etching that mark the early Eocene interval [3] and/or disputes related to the taxonomy of *T. bramlettei*. *Rhombaster cuspis* as well as *T. bramlettei* were seen synonyms [44], yet some authors believed that they have different structure [2, 3]. *Rhombaster cuspis* and *T. bramlettei* are considered different in this study and the LCtO of *T. bramlettei* delineates the entry of Zone NP10 (Table).

Some authors documented the disappearance of *Tribrachiatus bramlettei* within Zone NP10, nearby vanishing of *T. contortus*, preceding the beginning of *T. orthostylus* [20]. Similar finding is documented in the present study, where *T. bramlettei* disappears in sample 42 whereas *T. contortus* disappear in sample 43 and *T. orthostylus* appears in sample 45 (Table).

The LO *Sphenolithus radians* is correlative to the HO of *Tribrachiatus contort.* Consequently, the former bioevent approximates Zone's NP10 top [34]. However, some authors viewed *S. radians* close the top of Zone NP11 [5]. At Nukhul, *S. radians* first occurs in sample 45 and synchronizes appearing of *T. orthostylus* (Table).

Through latest Paleocene, Fasciculiths radiated then disappeared slightly after radiation [28] and [37]. Consequently, the HO of fasciculiths can approximate Zone's NP10 lower limit [42]. At Nukhul, the disappearance of *F. tympaniformis* coincides with Zone's NP9 (Table). Yet *F. tympaniformis* crossed into Zone NP10 in various sections around the world (see [26]). Moreover, Kasem et al. [25] viewed *F. tympaniformis* commonly occurring up to the midst of Zone NP10 at G. Misheiti (Sinai). These inconsistent stratigraphic ranges are probably due to the disagreements in the delineation of the LO of *T. bramlettei* that marks Zone's NP10 base of. These make it hard to infer whether it was survived, reworked, or its occurrences are diachronous.

Fasciculithus taxa that have their LOs in Zone NP9 were gathered by Agnini et al. [4] into *F. richardii* group. They delineated Zone's CNE1 limits utilizing the HOs of *F. richardii* group as well as *F. tympaniformis*, respectively. Disappearance of *F. alanii* and the first appearance of *Rhombosphaera calcitrapa*, *R. intermedia*, and *Rhabdosphaera solus* (*Blackites herculesii* herein) was utilized by Faris and Salem [21] to recognize Subzone's NP9b start. Furthermore, vanishing of *F. alanii* synchronizes Subzone's NP9b base as viewed by Abu Shama et al. [1], but it vanishes shortly before this time at the Dababiya GSSP [18]. At the Nukhul section, *F. alanii*, *F. thomasi*, *F. lillianiae* and *F. mitreus* vanishes within the bottom of Subzone NP9b, while the disappearance of *F. tympaniformis* synchronizes Subzone's NP9b top (Table).

Kasem et al. [25, 26] documented that *Zygrhablithus bijugatus* first occurs in coincidence with the start of Eocene. Yet it first occurs closely above this time at Nukhul (Table). *Discoaster mahmoudii* start occurring in subzone NP9b at Nukhul (Table). Several studies recorded *D. mahmoudii* in Zone NP9 [3]. *Discoaster mahmoudii* occurs at ~3.5 m, ~2 m and 7 m up the CIE at Dababiya, Oweina and Nezzi sections, respectively [29] and [18]. At Nukhul, *D. mahmoudii* occurs ~2 m overhead Eocene's base (Fig. 2). This confirms its unreliability in biostratigraphy.

Aubry and Salem [6] delineated Subzone NP9c from the HO of CNET to the LO of *Tribrachiatos bramlettei*. However, the RD taxa ranges up to Subzone NP10b [26]. Similar finding was documented in the present study (Table).

Blackites herculesii had been viewed in Zone NP9 in various localities in Egypt [26] and extends into Zone NP10 in other section [25, 26]. At Nukhul, *B. herculesii* first exists close to the lowest occurrence of *D. mahmoudii* in Subzone NP9b (Table). The increase in frequency of *Neochiastozygus junctus* was considered valuable in the delineation of the beginning of Zone NP10 as suggested by Abu Shama et al. [1]. In this study, *N. junctus* appears at Subzone's NP9b base and rises close to its top.

Discoaster binodosus can approximate Zone's NP9 top [34]. Yet Faris and Salem [21] viewed it close to the base of Subzone NP9b. Moreover, Kasem et al. [26] viewed *D. binodosus* in Zone NP10. At Nukhul, *D. binodosus* first appears just below Zone's NP9 top (Table). Thus, the LO of *D. binodosus* is considered insignificant biostratigraphic event [25].

Discoaster multiradiatus is presupposed to disappear in Zone NP11 according to Perch-Nielsen [34]. Yet its disappearance was recorded within Subzone NP10b [25]. Moreover, it disappears in sample 54 and its vanishing synchronizes the top of Zone NP11 at Nukhul (Table). These inconsistencies are probably due to reworking.

An acme of *Ericsonia subpertusa* accompanies the CIE at Dababiya [18]. At Nukhul, *E. subpertusa* is very abundant around the P/E boundary (Table). It is considered

warm-water taxa [16], and [13]. Perch-Nielsen [34] mentioned that calcareous nannoplanktons reach topmost diversification during late Paleocene. This is confirmed in this work, where most Paleocene *Fasciculithus* and *Discoaster* taxa (e.g., *F. thomasi*, *F. schaubii*, *F. alanii*, *F. lillianiae*, *F. richardi*, *F. mitreus*, *Discoaster multiradiatus*, *D. falcatus*, and *D. mediusus*) appear in Subzone NP9a (Table). Furthermore, several taxa first occur in this subzone including *Toweius callosus*, *Campylosphaera dela*, *Ellipsolithus distichus*, *Cyclagelosphaera reinhardti*, *Neochiastozygus junctus*, *Sphenolithus anarrhopus*, *Lophodolithus nascens* (Table).

The $\delta^{18}\text{O}$ and $\delta^{13}\text{C}$ isotopic changes were controlled by the isotope composition and temperature of sea water [39]. Therefore, they are significant for tracking variations in the water temperatures as well as changes in biogenic and oceanographic conditions. Negative $\delta^{13}\text{C}$ and $\delta^{18}\text{O}$ excursions were documented at the P/E limit at Dababiya, and is documented globally [18]. At Nukhul, $\delta^{13}\text{C}$ values decreases abruptly from 1.1 ‰ in sample 17 to 0.74 ‰ in sample 18 and -1.3 ‰ in sample 19 then increases gradually (Fig. 3). Similarly, the $\delta^{18}\text{O}$ values abruptly drop from -2.8 ‰ in sample 17 to -5.2 ‰ in sample 18 (Fig. 3). These abrupt decreases are due to climatic changes that associated the PETM. Eocene's base is also associated with a global fall in the carbonate content as documented by Dupuis et al. [18]. At Nukhul, it decreases from 52.5% just beneath the P/E boundary (sample 16) to 40.2% in sample 17 (the base of Eocene) and 55% in sample 19 (Fig. 3). This decrease in carbonate content probably resulted from sea level regression, which is evident by the common abundance of *Campylosphaera dela* and *Rhombosphaera* spp. that indicate shallow-water conditions [16]. Furthermore, it may result from a global decline in isotopes of carbon, a decline in productivity, a global ocean circulation changing, and/or a carbonate compensation depth's shoaling (CCD) [36], and [45].

6 Conclusion

In conclusion, the investigation of calcareous nannofossils, isotopic ratios ($\delta^{18}\text{O}$, $\delta^{13}\text{C}$), and carbonate content across the Paleocene-Eocene transition at Nukhul has provided valuable insights into the stratigraphic and paleoclimatic changes during this critical geological interval. Zones NP7/8 through NP12 were identified, along with the subdivision of Zone NP9 into two subzones and Zone NP10 into two subzones. This highlights the complex biostratigraphic framework at Nukhul. The overlapping ranges of *Tribrachiatos bramlettei*, *T. contortus*, and *T. orthostylus*, as well as the correlations between the appearances and disappearances of *Sphenolithus radians* and *T. contortus*, offer significant markers for stratigraphic assessment. However, the disappearance of *Fasciculithus tympaniformis* within

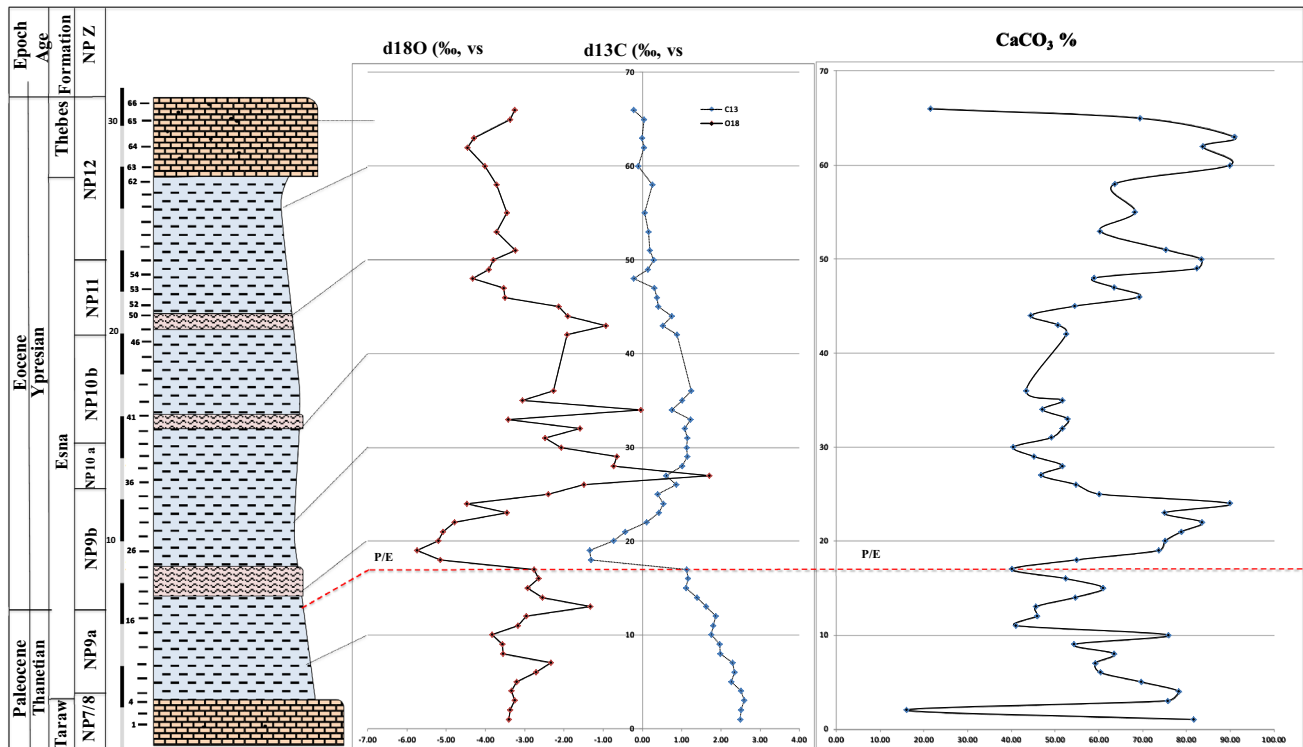


Fig. 3 Variations of $\delta^{13}\text{C}$, $\delta^{18}\text{O}$ and carbonate content of the late Paleocene-early Eocene sequence at the Nukhul section, West Central Sinai, Egypt

Subzone NP9b underscores the challenges in establishing precise boundaries, likely stemming from disagreements in the placement of the LO of *T. bramlettei* and the base of Zone NP10. Further complexities arise with the vanishing of several *Fasciculithus* species within Subzone NP9b and the uncertain biostratigraphic reliability of *Discoaster mahmoudii*'s appearance in the same subzone. Notably, the LO of *Neochiastozygus junctus* coinciding with the base of Subzone NP9b and the increasing abundance of *N. junctus* towards the subzone's top offer additional clues for refining the stratigraphy. *Discoaster binodosus*, though considered insignificant as a biostratigraphic event, appears just below the top of Zone NP9. The increased frequency of

Ericsonia subpervusa near the Paleocene-Eocene boundary is indicative of a warming event. Importantly, at Nukhul, this boundary was situated within the Esna Formation without significant lithological variations. Concurrently, the study documents global decreases in calcium carbonate content, $\delta^{13}\text{C}$ and $\delta^{18}\text{O}$ across the Paleocene-Eocene boundary, highlighting the broader climatic and environmental changes during this pivotal geological transition. These findings contribute to our understanding of the Paleocene-Eocene transition's complexity and provide essential data for future paleoclimatic and stratigraphic studies.

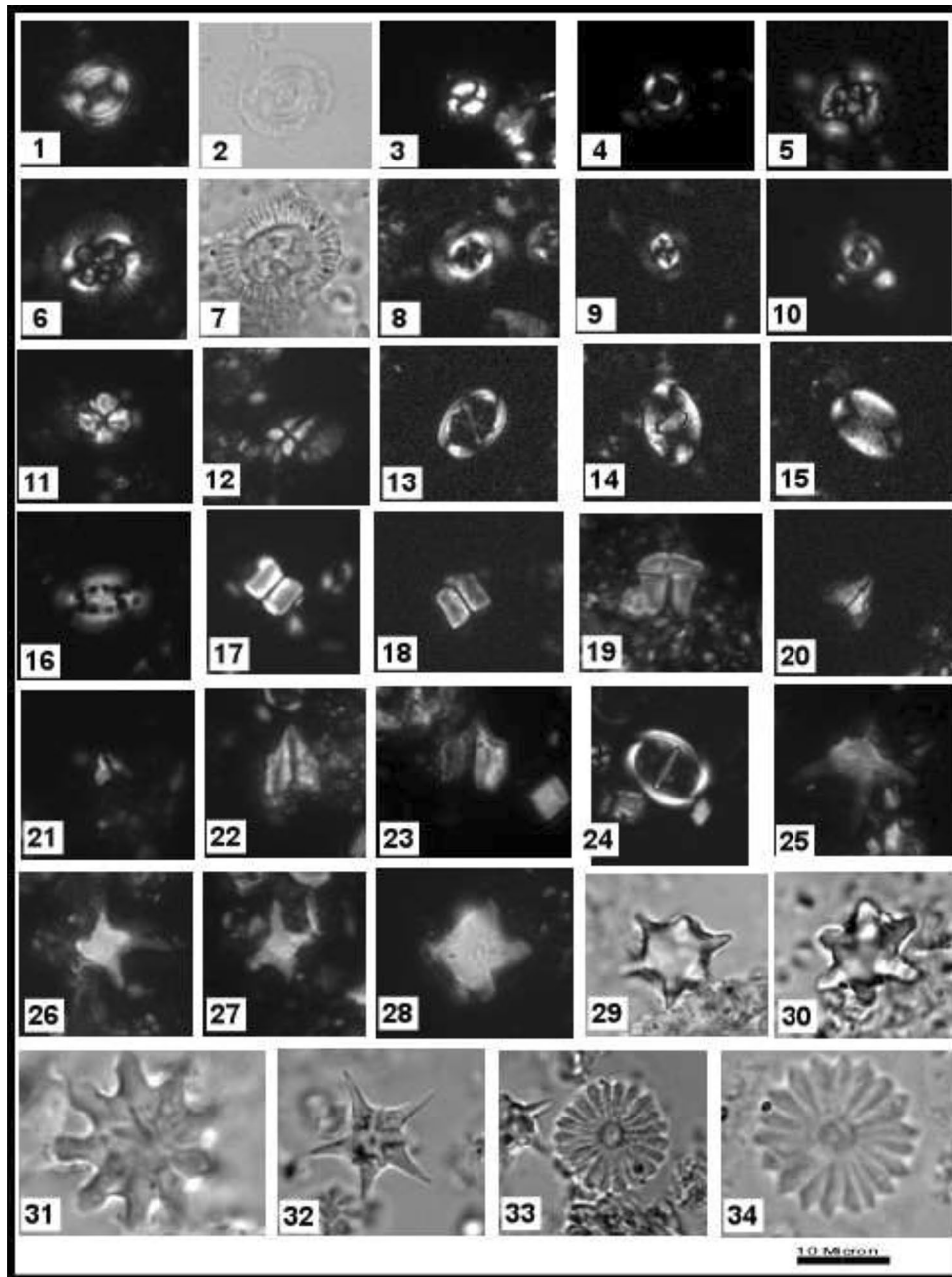


Plate 1, 2 *Ericsonia subpertusa*. Sample Number 11, Subzone NP9a. 3 *Coccolithus pelagicus*. Sample Number 11, Subzone NP9a. 4 *Ericsonia robusta*. Sample Number 11, Subzone NP9a. 5 *Cruciplacolithus tenuis*. Sample Number 17, Subzone NP9b. 6, 7 *Chiasmolithus consuetus*. Sample Number 6, Subzone NP9a. 8, 9 *Toweius pertusus*. Sample Number 6, Subzone NP9a. 10 *Toweius callosus*. Sample Number 11, Subzone NP9a. 11 *Sphenolithus primus*. Sample Number 6, Subzone NP9a. 12 *Sphenolithus radians*. Sample Number 54, Zone NP11. 13 *Neochiastozygus junctus*. Sample Number 30, Subzone NP9b. 14 *Helicosphaera seminulum*. Sample Number 38, Subzone NP10a. 15 *Pontosphaera plana*. Sample Number 42, Subzone NP10b. 16 *Ellipsolithus distichus* Sample Number 32, Sub-

zone NP9b. 17 *Fasciculithus involutus*. Sample Number 6, Subzone NP9a. 18 *Fasciculithus tympaniformis*. Sample Number 6, Subzone NP9a. 19 *Lithoptychius stegastos*. Sample Number 8, Subzone NP9a. 20, 21 *Fasciculithus alanii*. Sample Number 11, Subzone NP9a. 22, 23 *Fasciculithus lillianiae*. Sample Number 15, Subzone NP9a. 24 *Lophodolichus nascens*. Sample Number 41, Subzone NP10b. 25-28 *Rhomboaster cuspis*. Sample Number 32, Subzone NP9b. 29, 30 *Tribrachiatum bramlettei*. Sample Number 38, Subzone NP10a. 31 *Discoaster binodosus*. Sample Number 39, Subzone NP10b. 32 *Discoaster mahmoudii*. Sample Number 31, Subzone NP9b. 33, 34 *Discoaster multiradiatus*. Sample Number 16, Subzone NP9a.

Acknowledgements We are grateful to Prof. Dr. Sherwood Wise, Florida State University, USA, for his help throughout the investigation of the study section. Many thanks are also to five anonymous reviewers for their constructive comments and helpful suggestion to improve this manuscript.

Author contributions Material collection, field description, preparation, methodology and analyses were performed by AMK. Data curation, data interpretation, writing original draft, review & editing were carried out by AMK and WGK. Both authors have read and approved it.

Funding This research received no external funding.

Availability of data and material Materials are available at Calcareous Nannoplankton Lab at Geology Department, Faculty of Science, Damanhour University.

Declarations

Conflict of interest The authors declare no conflict of interest.

Open Access This article is licensed under a Creative Commons Attribution 4.0 International License, which permits use, sharing, adaptation, distribution and reproduction in any medium or format, as long as you give appropriate credit to the original author(s) and the source, provide a link to the Creative Commons licence, and indicate if changes were made. The images or other third party material in this article are included in the article's Creative Commons licence, unless indicated otherwise in a credit line to the material. If material is not included in the article's Creative Commons licence and your intended use is not permitted by statutory regulation or exceeds the permitted use, you will need to obtain permission directly from the copyright holder. To view a copy of this licence, visit <http://creativecommons.org/licenses/by/4.0/>.

References

1. Abu Shama A, Faris M, Al-Wosabi K (2007) Upper Paleocene–lower Eocene calcareous nannofossil biostratigraphy and paleoecology of Gebel Matulla section, Southwestern Sinai, Egypt. In: Proceedings of the 5th International Conference on the Geology of Africa, Assiut, Egypt, pp 33–51
2. Agnini C, Fornaciari E, Rio D, Tateo F, Backman J, Giusberti L (2007) Responses of calcareous nannofossil assemblages, mineralogy and geochemistry to the environmental perturbations across the Paleocene/Eocene boundary in the Venetian Pre-Alps. *Mar Micropaleontol* 63:19–38. <https://doi.org/10.1016/j.marmicro.2006.10.002>
3. Agnini C, Fornaciari E, Raffi I, Rio D, Röhl U, Westerhold T (2007) High-resolution nannofossil biochronology of middle Paleocene to early Eocene at ODP Site 1262: implications for calcareous nannoplankton evolution. *Mar Micropaleontol* 64:215–248. <https://doi.org/10.1016/j.marmicro.2007.05.003>
4. Agnini C, Fornaciari E, Raffi I, Catanzariti R, Pälke H et al (2014) Biozonation and biochronology of Paleogene calcareous nannofossils from low and middle latitudes. *Newslett Stratigr Stuttg* 47(2):131–181. <https://doi.org/10.1127/0078-0421/2014/0042>
5. Al Wosabi KA (2015) Calcareous nannofossils biostratigraphy and paleoecology of the late Paleocene/early Eocene of Wadi Nukhul West Central Sinai Egypt. *Earth Sci* 4(2):59–71. <https://doi.org/10.11648/j.earth.20150402.11>
6. Aubry M-P, Salem R (2013) The dababiya quarry core: coccolith biostratigraphy. *Stratigraphy* 9:241–259
7. Aubry M-P, Salem R (2013) The Dababiya Core: a window into Paleocene to early Eocene depositional history in Egypt based on coccolith stratigraphy. *Stratigraphy* 9:287–346
8. Aubry M-P, Berggren WA, Cramer B, Dupuis C, Kent DV et al. (1999) Paleocene/Eocene boundary sections in Egypt. In: Late Paleocene–Early Eocene Events from Northern Africa to the Middle East. International Symposium in connection with 1st International Conference on the Geology of Africa, Assiut, Egypt, pp 1–11
9. Aubry M-P, Ouda K, Dupuis C, Berggren WA, Van Couvering JA, Members of the Working Group on the Paleocene/Eocene Boundary (2007) The global standard stratotype-section and point (GSSP) for the base of the Eocene series in the Dababiya section (Egypt). *Episodes* 30(4):271–286. <https://doi.org/10.18814/epiugs/2007/v30i4/003>
10. Awad GH, and Ghobrial MG (1965) Zonal stratigraphy of the Kharga Oasis. Ministry of Industry, General Egyptian Organization for Geological Research and Mining, Geological Survey, Cairo, Egypt, paper no. 34:1–77
11. Bains S, Corfield RM, Norris RD (1999) Mechanisms of climate warming at the end of the Paleocene. *Science* 285(1999):724–727. <https://doi.org/10.1126/science.285.5428.724>
12. Beadnell HJL (1905) The relation of the Eocene and cretaceous systems in the Esna-Aswan Reach of the Nile-Valley. *J Geol Soc (Lond)* 61:667–676. <https://doi.org/10.1144/GSL.JGS.1905.061.01-04.35>
13. Bown PR, Pearson P (2009) Calcareous plankton evolution and the Paleocene/Eocene thermal maximum event: new evidence from Tanzania. *Mar Micropaleontol* 71:60–70. <https://doi.org/10.1016/j.marmicro.2009.01.005>
14. Bramlette MN, Sullivan FR (1961) Coccolithophorids and related nannoplankton of the early Tertiary in California. *Micropaleontology* 7:129–188
15. Brönnimann P, Stradner H (1960) Die foraminiferen und discoasteridenzonen von Kuba und ihre intercontinental correlation. *Erdoel* 76:364–369 (in German)
16. Bukry D (1973) Low latitude coccoliths biostratigraphic zonation. Initial Reports of the Deep Sea Drilling Project, 15: 685–703, US Government Printing Office, Washington
17. Copen TB (1996) More uncertainty than necessary. *Paleoceanography* 11(1996):369–370
18. Dupuis C, Aubry M-P, Steurbaut E, Berggren WA, Ouda K et al (2003) The Dababiya quarry section: lithostratigraphy, clay mineralogy, geochemistry and paleontology. *Micropaleontology* 49(2003):41–59. https://doi.org/10.2113/49.Suppl_1.41
19. Engleman EE, Jackson LL, Norton DR (1985) Determination of carbonate carbon in geological materials by coulometric titration. *Chem Geol* 53:125–128
20. Faris M (1997) Biostratigraphy of calcareous nannofossils across the K/T boundary in Egypt. *Neues Jb Geol Paläontol Abh* 5(1997):447–464
21. Faris M, and Salem R (2007) Paleocene–Eocene calcareous nannofossil biostratigraphy in west central Sinai, Egypt. In: Proceedings of the 8th Conference of Geology of Sinai for Development Ismailia, Egypt, pp 1–14
22. Faris M, Ghandour IM, Zahran E, Mosa G (2015) Calcareous nannoplankton changes during the Paleocene–Eocene thermal maximum in West Central Sinai Egypt. *Turk J Earth Sci* 24(5):475–493. <https://doi.org/10.3906/yer-1412-34>
23. Hay WW (1964) Utilisation stratigraphique des DISCOASTERIDES pour la zonation du Paleocene et de L'Eocene inferieur. *Mem. B.R.G.-M.*, 28, pp 885–889

24. Hay WW, Mohler HP (1967) Calcareous nannoplankton from early Tertiary rocks at Pont Labau, France, and Paleocene–early Eocene correlations. *J Paleontol* 41(6):1505–1541
25. Kasem AM, Wise S Jr, Faris M, Farouk S, Zahran E (2020) Upper Paleocene–lower Eocene calcareous nannofossil stratigraphy at the Mischeiti section, Central Sinai, Egypt. *Turk J Earth Sci* 29:242–256. <https://doi.org/10.3906/yer-1812-13>
26. Kasem AM, Wise S Jr, Faris M, Farouk S, Zahran E (2020) Calcareous nannofossil stratigraphy across the Paleocene/Eocene transition at the Gunnah section, Farafrā Oasis, Western Desert Egypt. *J Geol* 2020(128):371–387. <https://doi.org/10.1086/709359>
27. Kasem AM, Faris MM, Osman OM, Badawy AYE, Shaker F (2022) Calcareous nannofossil biostratigraphy and paleoenvironmental variations across the upper Paleocene–lowermost Eocene at Gebel Nezzazat, West Central Sinai Egypt. *Arab J Geosci* 15(8):688. <https://doi.org/10.1007/s12517-022-09763-3>
28. Martini E (1971) Standard Tertiary and Quaternary calcareous nannoplankton zonation. In: Farinacci A (ed) *Proceedings of the 2nd Planktonic Conference, Roma, Italy, (1970)*, pp 739–785
29. Monechi S, Angori E, and Speijer RP (2000) Upper Paleocene biostratigraphy in the Mediterranean region: Zonal markers, diachronism, and preservational problems. In: Andreasson FP, Schmitz B, Thompson EI (eds) *Early Paleogene warm climates and biosphere dynamics*, GFF, 122: 108–110. <https://doi.org/10.1080/11035890001221108>
30. Mutterlose J, Linnert C, Norris R (2007) Calcareous nannofossils from the Paleocene-Eocene thermal maximum of the equatorial Atlantic (ODP Site 1260B): evidence for tropical warming. *Mar Micropaleontol* 65(2007):13–31
31. Orabi OH, Hamad MM, Abu Saima MM (2023a) Foraminifera dissolution phases in the upper cretaceous succession of Jebel Duwi Egypt. *J Umm Al-Qura Univ Appl Sci* 9:1–19
32. Orabi OH, El-Sabbagh A, Mansour AS, Ismail H, Taha S (2023) Foraminifera study for the characterization of the Campanian/Maastrichtian boundary in Gebel Owaina Nile Valley Egypt. *J Umm Al-Qura Univ Appl Sci*. <https://doi.org/10.1007/s43994-023-00043-8>
33. Ouda KH, Berggren WA, Abdel Sabour A (2016) Upper Palaeocene–Lower Eocene biostratigraphy of Darb Gaga, Southeastern Kharga Oasis Western Desert. *Egypt J Afr Earth Sci* 118:12–23
34. Perch-Nielsen K (1985) Mesozoic calcareous nannofossils. In: Bolli S, Perch-Nielsen K (eds) *Plankton stratigraphy*. Cambridge University Press, Cambridge, pp 329–426
35. Raffi I, Backman J, Pälike H (2005) Changes in calcareous nannofossil assemblage across the Paleocene/Eocene transition from the paleo-equatorial Pacific Ocean. *Palaeogeogr Palaeoclimatol Palaeoecol* 226:93–126. <https://doi.org/10.1016/j.palaeo.2005.05.006>
36. Rea DK, Zachos JC, Owen RM, Gingerich PD (1990) Global change at the Paleocene-Eocene boundary: climatic and evolutionary consequences of tectonic events. *Palaeogeogr Palaeoclimatol Palaeoecol* 79(1990):117–128
37. Romein AJT (1979) Lineages in Early Paleocene nannoplankton. *Utrecht Micropaleontol Bull* 22:18–22
38. Said R (1960) Planktonic foraminifera from the Thebes Formation, Luxor Egypt. *Micropaleontology* 6:277–286. <https://doi.org/10.2307/1484234>
39. Shaaban MN (1997) Stable isotopes stratigraphy across the K/T boundary, and isotopic investigations of an “Ignored” Worm Bed, Eastern Desert Egypt. *Facies* 37:137–146
40. Shaker F, Kassab W (2022) Calcareous nannofossil biostratigraphy and paleoenvironmental study along the Upper Maastrichtian–Eocene sequence at Eastern and Western Deserts Egypt. *J Afr Earth Sci* 193:104583
41. Tantawy A (1998) *Stratigraphical and Paleocological Studies on Some Paleocene–Eocene Successions in Egypt*. Unpub. Ph.D. Thesis, Aswan Fac. Sci., South Valley Univ., Egypt, pp 273
42. Tantawy A (2006) Calcareous nannofossil of the Paleocene–Eocene transition at Qena Region, Central Nile Valley Egypt. *Micropaleontology* 52(3):193–222. <https://doi.org/10.2113/gsmicropal.52.3.193>
43. Thomas E, Zachos JC, Bralower TJ (2000) Ice-free to glacial world transition as recorded by benthic foraminifera. In: Huber BT, MacLeod KG, Wing SL (eds) *Warm climates in earth history*. Cambridge University Press, Cambridge, pp 132–160
44. Von Salis K, Monechi S, Bybell LM, Self-Trail J, Young JR (2000) Remarks on the calcareous nannofossil genera *Rhombaster* and *Tribrachiatatus* around the Paleocene/Eocene boundary. *Early Paleogene warm climates and biosphere dynamics*. GFF 122:138–140. <https://doi.org/10.1080/11035890001221138>
45. Zachos JC, Röhl U, Schellenberg SA, Sluijs A, Hodell DA, Kelly DC, Thomas E, Nicolo M, Raffi I, Lourens LJ, McCarren H, Kroon D (2005) Rapid acidification of the ocean during the Paleocene–Eocene Thermal Maximum. *Science* 308(2005):1611–1615

Publisher's Note Springer Nature remains neutral with regard to jurisdictional claims in published maps and institutional affiliations.